YAP/TAZ mediate TGFβ2-induced Schlemm's canal cell dysfunction

Haiyan Li[a,b,c], Kristin M. Perkumas[d], W. Daniel Stamer[d,e], Preethi S. Ganapathy[a,c,f], Samuel Herberg[a,b,c,g,h*]

Affiliations:

[a] Department of Ophthalmology and Visual Sciences, SUNY Upstate Medical University, Syracuse, NY 13210, USA

[b] Department of Cell and Developmental Biology, SUNY Upstate Medical University, Syracuse, NY 13210, USA

[c] BioInspired Institute, Syracuse University, Syracuse, NY 13244, USA

[d] Department of Ophthalmology, Duke Eye Center, Duke University, Durham, NC 27708, USA

[e] Department of Biomedical Engineering, Duke University, Durham, NC 27708, USA

[f] Department of Neuroscience and Physiology, SUNY Upstate Medical University, Syracuse, NY 13210, USA

[g] Department of Biochemistry and Molecular Biology, SUNY Upstate Medical University, Syracuse, NY 13210, USA

[h] Department of Biomedical and Chemical Engineering, Syracuse University, Syracuse, NY 13244, USA

*To whom correspondence should be addressed: Samuel Herberg, PhD, Assistant Professor; Department of Ophthalmology and Visual Sciences, SUNY Upstate Medical University, 505 Irving Avenue, Neuroscience Research Building Room 4609, Syracuse, NY 13210, USA, email: herbergs@upstate.edu

Keywords: POAG, mechanotransduction, TM stiffness, hydrogel, actin cytoskeleton

Abstract

Purpose: Elevated transforming growth factor beta2 (TGFβ2) levels in the aqueous humor have been linked to glaucomatous outflow tissue dysfunction. Potential mediators of dysfunction are the transcriptional co-activators, Yes-associated protein (YAP) and transcriptional coactivator with PDZ binding motif (TAZ). However, the molecular underpinnings of YAP/TAZ modulation in SC cells under glaucomatous conditions are not well understood. Here, we investigate how TGFβ2 regulates YAP/TAZ activity in human SC (HSC) cells using biomimetic extracellular matrix (ECM) hydrogels, and examine whether pharmacologic YAP/TAZ inhibition would attenuate TGFβ2-induced HSC cell dysfunction.

Methods: Primary HSC cells were seeded atop photocrosslinked ECM hydrogels, made of collagen type I, elastin-like polypeptide and hyaluronic acid, or encapsulated within the hydrogels. Changes in actin cytoskeleton, YAP/TAZ activity, ECM production, phospho-myosin light chain levels, and hydrogel contraction were assessed.

Results: TGFβ2 significantly increased YAP/TAZ nuclear localization in HSC cells, which was prevented by either filamentous (F)-actin relaxation or depolymerization. Pharmacologic YAP/TAZ inhibition using verteporfin decreased fibronectin expression and reduced actomyosin cytoskeletal rearrangement in HSC cells induced by TGFβ2. Similarly, verteporfin significantly attenuated TGFβ2-induced HSC cell-encapsulated hydrogel contraction.

Conclusions: Our data provide evidence for a pathologic role of aberrant YAP/TAZ signaling in HSC cells under simulated glaucomatous conditions, and suggest that pharmacologic YAP/TAZ inhibition has promising potential to improve outflow tissue dysfunction.

Introduction

The Schlemm's canal (SC) is a continuous vessel that encircles the anterior chamber at the iridocorneal angle; its lumen is lined with a single non-fenestrated layer of endothelial cells having both blood and lymphatic characteristics [1-5]. Situated in close apposition to the trabecular meshwork (TM), the SC is divided into the inner and outer wall [2]. The SC inner wall experiences a basal-to-apical pressure gradient (intraocular versus episcleral venous pressures) that drives aqueous humor into the SC lumen, which is then drained into the collector channels and aqueous veins [6]. Most of the resistance to aqueous humor outflow is generated at, or close to the SC inner wall in a region called the juxtacanalicular tissue (JCT) of the TM [7-9]. Importantly, increased outflow resistance in the JCT leads to elevated intraocular pressure (IOP), the only modifiable risk factor for primary open-angle glaucoma (POAG) [8, 10-13].

Previous studies have demonstrated that glaucomatous SC cells isolated from POAG eyes exhibited higher levels of filamentous (F)-actin, α-smooth muscle actin (αSMA) and fibronectin, as well as increased cell stiffness compared to normal SC cells [14, 15]. The ocular hypertension-causing steroid dexamethasone was shown to increase F-actin fibers, while the IOP-lowering Rho-associated kinase (ROCK) inhibitor Y27632 decreased F-actin levels [16, 17]; F-actin is thought to mediate SC cell contractility and stiffness to negatively affect aqueous humor outflow and IOP [18]. Thus, SC cell dysfunction is thought to be a significant contributor to the increased outflow resistance in POAG; however, the mechanistic underpinnings of SC cell pathobiology remain incompletely understood.

Transforming growth factor beta 2 (TGFβ2), the predominant TGFβ isoform in the eye and aqueous humor, is a major player in contributing to the pathologic changes in POAG [10, 19-23]. It has been shown that levels of TGFβ2 are elevated in eyes of glaucoma patients compared to age-

matched normal eyes [21, 22, 24, 25]. In culture, TM and SC cells isolated from donor eyes with POAG secrete more active TGFβ2 protein compared to normal cells [15, 26]. Accordingly, perfusion of TGFβ2 in human anterior segments increases resistance in the conventional outflow pathway [27]. At the cellular level, TGFβ2 increases actin stress fibers and phospho-myosin light chain (p-MLC) to drive pathologic TM cell contraction [28-30]. Moreover, exposure of TM cells to TGFβ2 induces the expression/deposition of extracellular matrix (ECM) proteins such as collagen types I and IV, and fibronectin [28, 31-33]. Despite the progress made in uncovering the role of TGFβ2 in TM cell dysfunction, the contributions of TGFβ2 to SC cell pathobiology are less well understood.

Yes-associated protein (YAP) and transcriptional coactivator with PDZ-binding motif (TAZ) are powerful regulators of cell proliferation and differentiation, with an established link to tissue fibrosis [34-38]. Upon nuclear translocation, YAP/TAZ interact with TEA domain (TEAD) transcription factors to drive the expression of known (CTGF, CYR61, ANKRD1) and glaucoma-related putative downstream effectors of active YAP/TAZ signaling (e.g., transglutaminase-2 (TGM2)) [39]. To that end, *YAP1* was recently identified among a group of previously unknown POAG risk loci across European, Asian and African ancestries, suggesting a potential causal association with outflow dysfunction [40]. YAP/TAZ can be activated by multiple stimuli, such as stiffened ECM, increased mechanical stress, and exposure to growth factors [41, 42]. Recently, we demonstrated that both ECM stiffening and TGFβ2 increase YAP/TAZ activity in human TM cells, which was linked to pathologic cell contractility and ECM remodeling that may exacerbate glaucoma pathology [26].

The physiological substrate of the SC inner wall endothelial cells is its discontinuous basal lamina, which is in direct contact with the JCT [3, 6]. Recently, we developed a bioengineered hydrogel composed of ECM biopolymers found in the native JCT region encapsulated with human

TM (HTM) cells, and demonstrated its utility for studying cell-ECM interactions under normal and simulated glaucomatous conditions in a relevant tissue-mimetic 3D microenvironment [26, 30, 43]. Here, we investigated the effects of TGFβ2 on regulating YAP/TAZ activity in human SC (HSC) cells cultured atop the acellular ECM hydrogel. Additionally, we examined whether pharmacologic YAP/TAZ inhibition would alleviate TGFβ2-induced HSC cell dysfunction.

Materials and Methods

HSC cell isolation and culture

Experiments using human donor eye tissue were approved by the SUNY Upstate Medical University Institutional Review Board (protocol #1211036), and were performed in accordance with the tenets of the Declaration of Helsinki for the use of human tissue. Primary HSC cells were isolated from healthy donor corneal rims discarded after transplant surgery and cultured according to established protocols [5]. Briefly, the corneal rims were cut into wedges and placed into a 100 mm dish containing low-glucose Dulbecco's Modified Eagle's Medium (DMEM; Gibco; Thermo Fisher Scientific, Waltham, MA, USA) with 10% fetal bovine serum (FBS; Atlanta Biologicals, Flowery Branch, GA, USA) and 1% penicillin/streptomycin/glutamine (PSG; Gibco). Using an SMZ1270 stereomicroscope (Nikon Instruments, Melville, NY, USA), a 2% gelatin-coated (Sigma-Aldrich) 6-0 nylon monofilament sterile suture (eSutures, Mokena, IL, USA) was inserted into the SC lumen of each wedge with fine-tipped forceps (Fine Science Tools, Foster City, CA, USA), and these wedges were cultured in DMEM with 10% FBS and 1% PSG, and maintained at 37°C in a humidified atmosphere with 5% CO_2 for 3 weeks. Next, curvilinear incisions were made parallel to Schwalbe's line (alongside the suture) into the TM, which produced a TM flap. After lifting the TM, the sutures were gently removed, and a ~2 mm long piece was cut from each end

of the suture to prevent fibrotic cell contamination. Next, the sutures were washed with Dulbecco's Phosphate Buffered Saline (DPBS; Gibco), placed into a single well of gelatin-coated (Sigma-Aldrich) 6-well culture plates (Corning; Thermo Fisher Scientific), and digested for 2 min with 0.25% trypsin/0.5 mM EDTA (Gibco). Subsequently, 5 ml DMEM with 10% FBS and 1% PSG were added, and the sutures were moved to another gelatin-coated well. The digests and sutures were cultured in DMEM with 10% FBS and 1% PSG, and maintained at 37°C in a humidified atmosphere with 5% CO_2. Fresh media was supplied every 2-3 days. Once confluent, HSC cells were lifted with 0.25% trypsin/0.5 mM EDTA and sub-cultured in DMEM with 10% FBS and 1% PSG. All studies were conducted using cells passage 3-6. Four HSC cell strains (HSC01, HSC02, HSC03, HSC09) were characterized and used for the experiments herein; the reference cell strain HSC78 was isolated and characterized at Duke University by K.M.P. and W.D.S. (**Table 1**). Different combinations of 2-3 HSC cell strains were used per experiment, depending on cell availability.

Table 1: HSC cell strain information.

ID	Sex	Age
HSC01	Male	33
HSC02	Male	46
HSC03	Female	46
HSC09	Female	69
Reference HSC78*	Male	77
**obtained from W.D.S. at Duke University*		

HSC cell characterization

HSC cells were seeded at 1×10^4 cells/cm^2 in 6-well culture plates or on sterilized glass coverslips in 24-well culture plates, and cultured in DMEM with 10% FBS and 1% PSG. HSC cell morphology and growth characteristics were monitored by phase contrast microscopy using an LMI-3000 Series Routine Inverted Microscope (Laxco; Thermo Fisher Scientific). Once confluent, monolayers of HSC cells were processed for immunocytochemistry and immunoblot analyses to assess expression of fibulin-2 and vascular endothelial-cadherin (VE-CAD), respectively. To rule out the contamination of HTM cells, dexamethasone (DEX; Fisher Scientific)-induced myocilin (MYOC) expression was assessed in HSC cells. Briefly, confluent HSC cells were treated with 100 nM DEX or vehicle control (0.1% (v/v) ethanol) in DMEM with 1% FBS and 1% PSG for 4 d, and serum- and phenol red-free DMEM for 3 d. The HSC cell culture supernatants were collected and concentrated using Amicon® Ultra Centrifugal Filters (Millipore Sigma, Burlington, MA, USA) for immunoblot analysis.

Preparation of ECM thin-film hydrogels

Hydrogel precursors methacrylate-conjugated bovine collagen type I (MA-COL, Advanced BioMatrix, Carlsbad, CA, USA; 3.6 mg/ml [all final concentrations]), thiol-conjugated hyaluronic acid (SH-HA, Glycosil®, Advanced BioMatrix; 0.5 mg/ml, 0.025% (w/v) photoinitiator Irgacure® 2959; Sigma-Aldrich, St. Louis, MO, USA) and in-house expressed elastin-like polypeptide (SH-ELP, thiol via KCTS flanks [43]; 2.5 mg/ml) were thoroughly mixed. Thirty microliters of the hydrogel solution were pipetted onto a Surfasil (Fisher Scientific)-coated 18 × 18-mm square glass coverslip followed by placing a regular 12-mm round glass coverslip onto the hydrogels. Constructs were crosslinked by exposure to UV light (OmniCure S1500 UV Spot Curing System;

Excelitas Technologies, Mississauga, Ontario, Canada) at 320-500 nm, 2.2 W/cm^2 for 5 s, as previously described [26, 30, 43]. The hydrogel-adhered coverslips were removed with fine-tipped tweezers and placed in 24-well culture plates (Corning; Thermo Fisher Scientific).

HSC cell treatments

HSC cells were seeded at 2 × 10^4 cells/cm^2 atop premade ECM hydrogels and cultured in DMEM with 10% FBS and 1% PSG for 1 or 2 days. Then, HSC cells were cultured in serum-free DMEM with 1% PSG and subjected to the different treatments for 3 d: TGFβ2 (2.5 ng/ml; R&D Systems, Minneapolis, MN, USA), the ROCK inhibitor Y27632 (10 μM; Sigma-Aldrich), the actin depolymerizer latrunculin B (10 μM; for 30 min only to preserve cell viability; Tocris Bioscience; Thermo Fisher Scientific), or the YAP inhibitor verteporfin (0.5 μM; Sigma).

Immunoblot analysis

Equal protein amounts (10 μg), determined by standard bicinchoninic acid assay (Pierce; Thermo Fisher Scientific), from HSC cell lysates in lysis buffer (CelLytic™ M, Sigma-Aldrich) or from concentrated HSC cell culture supernatants ± DEX at 7 d supplemented with Halt™ protease/phosphatase inhibitor cocktail (Thermo Fisher Scientific) in 4× loading buffer (Invitrogen; Thermo Fisher Scientific) with 5% beta-mercaptoethanol (Fisher Scientific) were boiled for 5 min, subjected to SDS-PAGE using NuPAGE™ 4-12% Bis-Tris Gels (Invitrogen; Thermo Fisher Scientific) at 120V for 80 min, and transferred to 0.45 μm PVDF membranes (Sigma; Thermo Fisher Scientific). Membranes were blocked with 5% bovine serum albumin (Thermo Fisher Scientific) in tris-buffered saline with 0.2% Tween®20 (Thermo Fisher Scientific), and probed with various primary antibodies followed by incubation with HRP-conjugated secondary

183 antibodies or fluorescent secondary antibodies (LI-COR, Lincoln, NE, USA). Bound antibodies
184 were visualized with the enhanced chemiluminescent detection system (Pierce) on
185 autoradiography film (Thermo Fisher Scientific) or Odyssey® CLx imager (LI-COR). A list of all
186 antibodies and their working dilutions can be found in **Supplementary Table 1**.
187
188 ***Immunocytochemistry analysis***
189 HSC cells atop ECM hydrogels subjected to the different treatments for 3 d were fixed with 4%
190 paraformaldehyde (Thermo Fisher Scientific) at room temperature for 20 min, permeabilized with
191 0.5% Triton™ X-100 (Thermo Fisher Scientific), blocked with blocking buffer (BioGeneX), and
192 incubated with primary antibodies, followed by incubation with fluorescent secondary antibodies;
193 nuclei were counterstained with 4′,6′-diamidino-2-phenylindole (DAPI; Abcam). Similarly, cells
194 were stained with Phalloidin-iFluor 488 (Invitrogen) or 594 (Abcam)/DAPI according to the
195 manufacturer's instructions. Coverslips were mounted with ProLong™ Gold Antifade (Invitrogen)
196 on Superfrost™ microscope slides (Fisher Scientific), and fluorescent images were acquired with
197 an Eclipse N*i* microscope (Nikon Instruments, Melville, NY, USA). A list of all antibodies and
198 their working dilutions can be found in **Supplementary Table 1**.
199
200 ***Image analysis***
201 All image analyses were performed using FIJI software (National Institutes of Health (NIH),
202 Bethesda, MD, USA). Briefly, the cytoplasmic YAP/TAZ intensity was measured by subtracting
203 the overlapping nuclear (DAPI) intensity from the total YAP/TAZ intensity. The nuclear
204 YAP/TAZ intensity was recorded as the proportion of total YAP/TAZ intensity that overlapped
205 with the nucleus (DAPI). YAP/TAZ nuclear/cytoplasmic (N/C) ratio was calculated as follows:

206 N/C ratio = (nuclear YAP/TAZ signal/area of nucleus)/(cytoplasmic signal/area of cytoplasm).
207 Fluorescence intensity of F-actin, FN, TGM2, and p-MLC were measured in at least 30 images
208 from 3 HSC cell strains with 3 replicates per HSC cell strain with image background subtraction
209 using FIJI software. Given the lack of defined αSMA fibers in untreated controls, we measured
210 the percent of αSMA-positive cells using FIJI software. At least 150 cells were analyzed in 30
211 images from 3 HSC cell strains with 3 replicates per HSC cell strain.
212
213 ***HSC hydrogel contraction analysis.***
214 HSC cell-laden hydrogels were prepared by mixing HSC cells (1.0×10^6 cells/ml) with MA-
215 COL (3.6 mg/ml), SH-HA (0.5 mg/ml, 0.025% (w/v) photoinitiator) and SH-ELP (2.5 mg/ml) on
216 ice, followed by pipetting 10 µl droplets of the HSC cell-laden hydrogel precursor solution onto
217 polydimethylsiloxane (PDMS; Sylgard 184; Dow Corning)-coated 24-well culture plates.
218 Constructs were crosslinked as described above (320-500 nm, 2.2 W/cm^2, 5 s). HSC cell-laden
219 hydrogels were cultured in DMEM with 10% FBS and 1% PSG in presence of the different
220 treatments. Longitudinal brightfield images were acquired at 0 d and 5 d with an Eclipse T*i*
221 microscope (Nikon). Construct area from N = 12 hydrogels per group from 3 HSC cell strains with
222 4 replicates per cell strain was measured using FIJI software and normalized to 0 d followed by
223 normalization to controls.
224
225 ***HSC hydrogel cell viability analysis***
226 Cell viability was measured with the CellTiter 96® Aqueous Non-Radioactive Cell
227 Proliferation Assay (Promega) following the manufacturer's protocol. HSC hydrogels cultured in
228 DMEM with 10% FBS and 1% PSG in presence of the different treatments for 5 d were incubated

with the staining solution (38 µl MTS, 2 µl PMS solution, 200 µl DMEM) at 37ºC for 1.5 h. Absorbance at 490 nm was recorded using a spectrophotometer plate reader (BioTek, Winooski, VT, USA). Blank-subtracted absorbance values served as a direct measure of HSC cell viability from N = 12 hydrogels per group from 3 HSC cell strains with 4 replicates per cell strain.

Statistical analysis

Individual sample sizes are specified in each figure caption. Comparisons between groups were assessed by two-way analysis of variance (ANOVA) with Tukey's multiple comparisons *post hoc* tests, as appropriate. The significance level was set at $p<0.05$ or lower. GraphPad Prism software v9.2 (GraphPad Software, La Jolla, CA, USA) was used for all analyses.

Results

HSC cell characterization

Four HSC cell strains (HSC01, HSC02, HSC03, and HSC09) were used and compared to a validated reference strain (HSC78). All of our HSC cell strains exhibited typical spindle-like elongated cell morphology comparable to the reference standard (**Fig. 1A**). A reliable feature of HSC cells *in vitro* is expression of two positive markers, fibulin-2 and vascular endothelial-cadherin (VE-CAD) [44]. Our results show that all HSC cell strains highly expressed fibulin-2 (**Fig. 1B**) and VE-CAD (**Fig. 1C**), comparable to the reference strain. In culture, HTM cells upregulate MYOC expression following challenge with the corticosteroid DEX [45], whereas this does not occur in HSC cells. We observed that none of the HSC cell strains expressed MYOC in response to DEX treatment (**Fig. 1D**), suggesting pure HSC cell preparations devoid of HTM cell contamination.

Together, these data suggest that HSC01, HSC02, HSC03, and HSC09 exhibit required key characteristics according to previous publications [5, 44] to faithfully identify them as normal HSC cells, comparable to a confirmed reference standard.

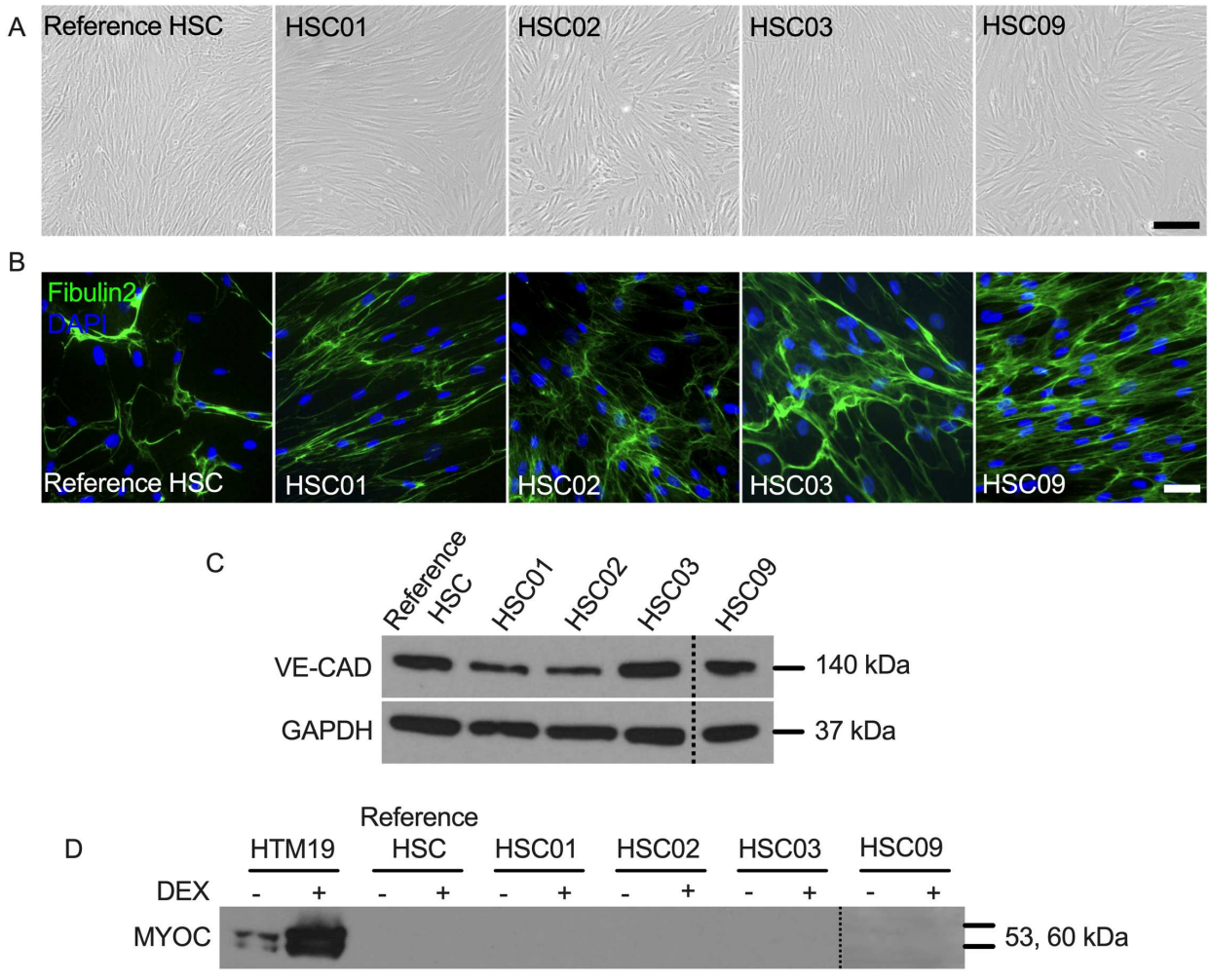

Fig. 1. HSC cell characterization. (A) Representative phase contrast micrographs of reference HSC, HSC01, HSC02, HSC03, and HSC09 cell strains. Scale bar, 200 µm. (B) Representative immunofluorescence micrographs of fibulin-2. Scale bar, 100 µm. (C) Immunoblot of VE-Cadherin (VE-CAD). (D) Immunoblot of secreted myocilin (MYOC) at 7 d (= negative marker).

Effects of TGFβ2 in the absence or presence of ROCK inhibition or Lat B on actin cytoskeleton in HSC cells.

F-actin levels are higher in SC cells isolated from POAG eyes compared to normal SC cells [15]. To investigate the effects of TGFβ2 on actin cytoskeleton remodeling, HSC cells were cultured atop premade ECM hydrogels and treated with TGFβ2 alone, or co-treated with ROCK inhibitor Y27632 or latrunculin B (Lat B), a compound that inhibits actin polymerization (**Fig. 2A**). We observed significantly increased F-actin fibers in HSC cells treated with TGFβ2 compared to controls, which was significantly prevented by co-treatment with Y27632 or Lat B co-treatment; with acute Lat B treatment showing a stronger effect (**Fig. 2B,C**). Of note, both types of actin destabilizers failed to fully block TGFβ2-induced F-actin assembly. We observed a range of responsiveness to the TGFβ2 challenge ± treatments among the HSC cell strains, indicating normal donor-to-donor viability.

We, and others, have shown that the fibrotic marker α-smooth muscle actin (αSMA) is upregulated in HTM cells by TGFβ2 exposure [28-30, 46]. Here, we demonstrated that TGFβ2 induced expression of αSMA in 45.87% of HSC cells compared to only ~3.16% in controls. Similar to results with F-actin, Y27632 prevented αSMA expression induced by TGFβ2, with only 13.98% αSMA^+ cells. Interestingly, short term Lat B treatment failed to block TGFβ2-induced αSMA expression (% of αSMA^+ cells: 41.95%) (**Fig. 2D,E**).

Collectively, these data demonstrate that TGFβ2 upregulates F-actin fibers in HSC cells, which is decreased by either actin cytoskeleton relaxation or depolymerization. Furthermore, TGFβ2 induces αSMA expression, which is prevented by ROCK inhibition, whereas short-term actin depolymerization does not influence aberrant αSMA stress fiber formation independent on the cell strain used.

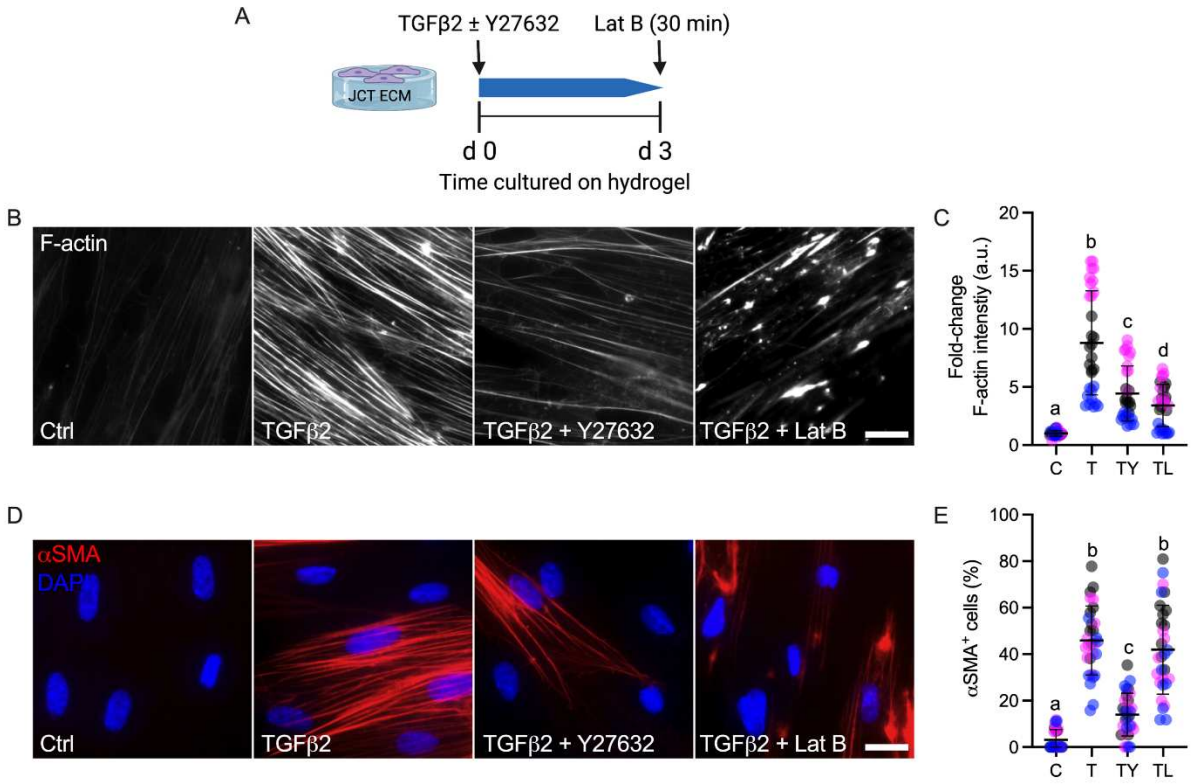

283

284 **Fig. 2. Effects of TGFβ2 in the absence or presence of a ROCK inhibitor or Lat B on F-actin**
285 **and αSMA stress fibers in HSC cells.** (A) Schematic showing time course of the different
286 treatments. (B) Representative fluorescence micrographs of F-actin in HSC cells on ECM hydrogel
287 substrates subjected to control, TGFβ2 (3 d; 2.5 ng/mL), TGFβ2 + Y27632 (3 d; 10 μM), TGFβ2
288 (3 d) + Lat B (30 min; 2 μM). Scale bar, 20 μm. (C) Analysis of F-actin intensity (N = 30 images
289 per group from 3 HSC cell strains with 3 replicates per HSC cell strain). (D) Representative
290 immunofluorescence micrographs of αSMA in HSC cells on ECM hydrogel substrates subjected
291 to the different treatments. Scale bar, 20 μm. (E) Analysis of percentage of αSMA^+ cells (N = 30
292 images per group from 3 HSC cell strains with 3 experimental replicates per HSC cell strain; more
293 than 150 cells were analyzed per cell strain). Symbols with different colors represent different cell
294 strains. The bars and error bars indicate Mean ± SD. Significance was determined by two-way
295 ANOVA using multiple comparisons tests (shared significance indicator letters represent non-
296 significant difference ($p>0.05$), distinct letters represent significant difference ($p<0.05$)).

297

298

TGFβ2 stabilizes actin cytoskeleton to upregulate YAP/TAZ activity

Recently, we demonstrated that TGFβ2 increases nuclear YAP and TAZ, a readout for active YAP/TAZ signaling, in HTM cells cultured atop or within ECM hydrogels [26]. To assess the effect of TGFβ2 on YAP/TAZ subcellular localization in HSC cells subjected to the different treatments, we evaluated both YAP and TAZ nuclear-to-cytoplasmic (N/C) ratios. We observed that exposure to TGFβ2 significantly increased YAP N/C ratio (**Fig. 3A,B**), TAZ N/C ratio (**Fig. 3C,D**), and expression of their putative downstream effector TGM2 (**Fig. 3E,F**) compared to controls; suggesting that TGFβ2 enhanced YAP/TAZ transcriptional activity. Given that actin cytoskeletal integrity is required for proper YAP/TAZ regulation in a variety of cells [41, 47], we investigated whether TGFβ2-induced YAP/TAZ activation in HSC cells depended on an intact actin cytoskeleton. Our results revealed that HSC cells co-treated with Y27632 or Lat B significantly decreased TGFβ2-induced YAP/TAZ nuclear localization and TGM2 expression. Consistent with our observation on F-actin fibers in response to the different treatments, Lat B was more effective in decreasing YAP/TAZ activity in HSC cells (i.e., below control levels) compared to Y27632 (**Fig. 3A-F**).

Together, these data show that TGFβ2 increases nuclear YAP/TAZ and TGM2 expression in HSC cells from multiple donors, which is potently attenuated by either actin cytoskeleton relaxation or depolymerization.

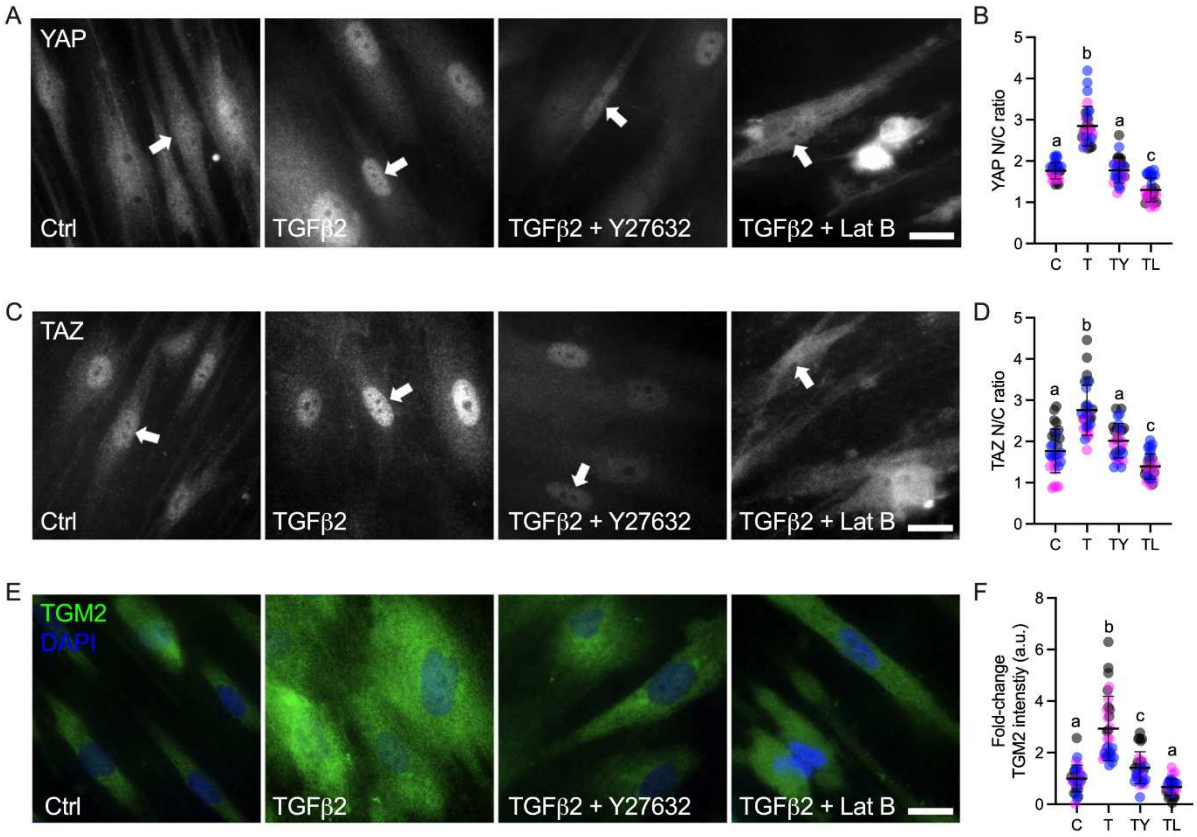

Fig. 3. Effects of TGFβ2 in the absence or presence of a ROCK inhibitor or Lat B on YAP/TAZ activity in HSC cells. (A and B) Representative immunofluorescence micrographs of YAP and TAZ in HSC cells on ECM hydrogel substrates subjected to control, TGFβ2 (3 d; 2.5 ng/mL), TGFβ2 + Y27632 (3 d; 10 μM), TGFβ2 (3 d) + Lat B (30 min; 2 μM). Scale bar, 20 μm; arrows indicate YAP/TAZ nuclear localization. (C and D) Analysis of YAP/TAZ nuclear/cytoplasmic ratio (N = 30 images from 3 HSC cell strains with 3 experimental replicates per cell strain). (E) Representative fluorescence micrographs of TGM2 in HSC cells on ECM hydrogel substrates subjected to the different treatments. Scale bar, 20 μm. (F) Analysis of TGM2 intensity (N = 30 images from 3 HSC cell strains with 3 replicates per cell strain). Symbols with different colors represent different cell strains. The bars and error bars indicate Mean ± SD. Significance was determined by two-way ANOVA using multiple comparisons tests (shared significance indicator letters represent non-significant difference ($p>0.05$), distinct letters represent significant difference ($p<0.05$)).

YAP/TAZ mediate ECM remodeling and actomyosin cell cytoskeleton

It has been shown that HSC cells isolated from glaucomatous eyes exhibit increased F-actin levels and expression of ECM proteins including fibronectin [15]; in this study, our results suggest that TGFβ2 also increases actin cytoskeleton remodeling. Both abnormal ECM deposition and

actin remodeling may be part of a pathologic signature in HSC cells. Therefore, we next tested whether pharmacologic YAP/TAZ inhibition could rescue TGFβ2-induced HSC cell dysfunction. To do so, HSC cells atop ECM hydrogels were treated with TGFβ2 alone or co-treated with verteporfin (VP), which disrupts nuclear YAP/TAZ-TEAD interactions thereby inhibiting transcriptional activity [48]. Co-treatment of VP with TGFβ2 significantly decreased N/C ratios of YAP and TAZ in HSC cells compared to TGFβ2 alone, approximating baseline levels (**Suppl. Fig. 1A-D**). Similarly, VP significantly decreased TGFβ2-stimulated TGM2 expression; yet, levels remained significantly higher compared to controls (**Suppl. Fig. 1E,F**).

We observed that exposure to VP significantly reduced TGFβ2-induced fibronectin deposition approximating untreated controls (**Fig. 4A,B**). Importantly, we demonstrated that TGFβ2-induced αSMA expression (**Fig. 4C,D**), F-actin fibers (**Fig. 4E,F**), and phospho-myosin light chain (p-MLC) levels (**Fig. 4G,H**) were significantly decreased by VP co-treatment, but again did not reach baseline levels.

In sum, these data suggest that pharmacologic YAP/TAZ inhibition reduces the expression of fibronectin and decreases actomyosin cytoskeletal rearrangement independent of the cell strain used.

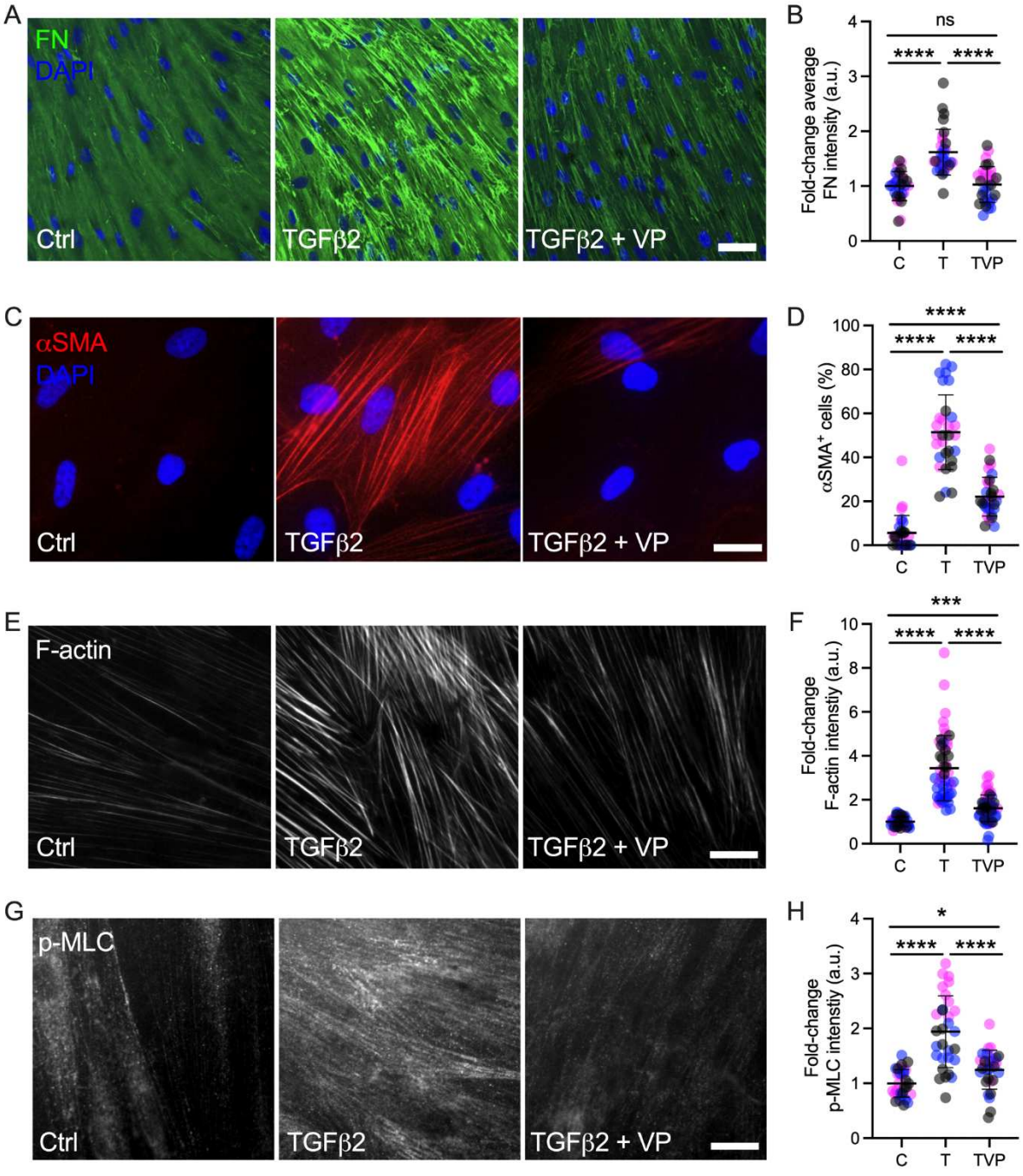

Fig. 4. Effects of YAP/TAZ inhibition on ECM remodeling and actomyosin cytoskeleton in HSC cells. (A) Representative immunofluorescence micrographs of fibronectin (FN) in HSC cells on ECM hydrogel substrates subjected to control, TGFβ2 (3 d; 2.5 ng/mL), TGFβ2 + VP (3 d; 0.5 μM). Scale bar, 100 μm. (B) Analysis of fibronectin intensity (N = 30 images per group from 3 HSC cell strains with 3 experimental replicates per HSC cell strain). (C) Representative immunofluorescence micrographs of αSMA in HSC cells on ECM hydrogel substrates subjected to the different treatments. Scale bar, 20 μm. (D) Analysis of percentage of αSMA^{+} cells (N = 3 HSC cells strains, more than 150 cells were analyzed per cell strain). (E and G) Representative

fluorescence micrographs of F-actin and p-MLC in HSC cells on ECM hydrogel substrates subjected to the different treatments. Scale bar, 20 μm. (F and H) Analysis of F-actin and p-MLC intensity (N = 30 images from 3 HSC cell strains with 3 experimental replicates per cell strain). Symbols with different colors represent different cell strains. The bars and error bars indicate Mean ± SD. Significance was determined by two-way ANOVA using multiple comparisons tests (*p<0.05, ***p<0.001, ****p < 0.0001).

YAP/TAZ mediate TGFβ2-induced HSC cell contractility

It has been shown that perfusing *ex vivo* human anterior segments with TGFβ2 reduced the length of the SC inner wall [27], suggestive of tissue contraction. HSC cells are known to be highly contractile [3]. To that end, we observed that HSC cell-laden hydrogels were markedly more contractile than comparable HTM cell-encapsulated hydrogels, reaching ~35-42% of their original size by 5 d with normal donor-to-donor variability (**Suppl. Fig.2**). Our data so far showed that YAP/TAZ inhibition reduced pathologic actomyosin cytoskeleton remodeling. Therefore, we hypothesized that TGFβ2 may increase HSC cell contractility, which could be reduced by YAP/TAZ inhibition. To test this hypothesis, we encapsulated HSC cells in ECM hydrogels - a method developed in our laboratory to characterize HTM cell behavior [26, 30, 43] - and treated the constructs with TGFβ2, either alone or in combination with VP, to assess the level of hydrogel contraction at 5 d. TGFβ2-treated HSC hydrogels exhibited significantly greater contraction compared to controls (62.79% of controls; **Fig. 5A,B**), consistent with our previous studies using HTM cells [26, 30, 43]. Co-treatment with VP significantly decreased pathologic HSC hydrogel contraction (81.56% of controls) compared to TGFβ2-treated samples (**Fig. 5A,B**), but it did not fully restore baseline levels. Of note, the influence of VP on HSC cell-laden hydrogel contraction differed between HSC cell strains, showing a stronger effect on HSC02 than HSC03 and HSC09 consistent with normal donor-to-donor variability (**Fig. 4A,B**). To rule out that hydrogel contractility was influenced by the cell number, we assessed HSC cell viability in constructs

subjected to the different treatments. No differences were observed for HSC cell-laden hydrogels across groups (**Fig. 5C**).

Together, these data demonstrate that TGFβ2 robustly induces HSC cell contractility in a 3D ECM microenvironment across multiple cell strains, and that pharmacologic YAP/TAZ inhibition potently decreases pathologic HSC cell contraction.

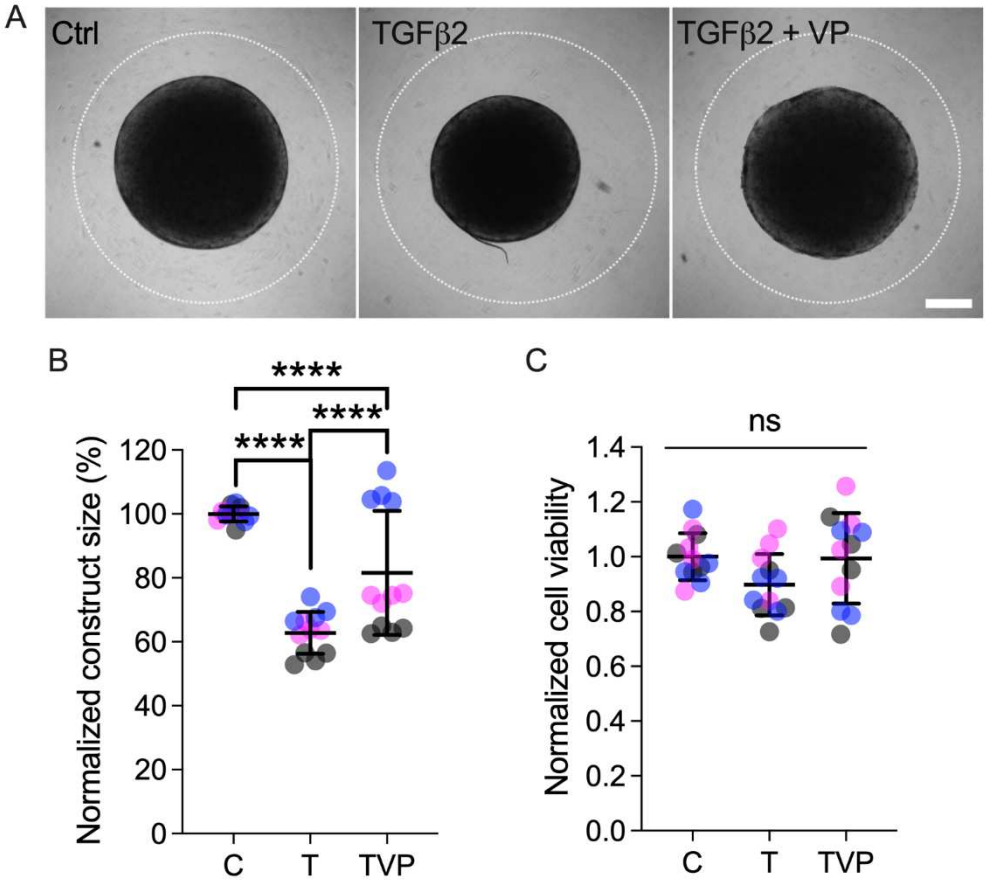

Fig. 5. Effects of TGFβ2 in the absence or presence of YAP/TAZ inhibition on HSC hydrogel contractility. (A) Representative brightfield images of HSC hydrogels subjected to control, TGFβ2 (3 d; 2.5 ng/mL), TGFβ2 + VP (3 d; 0.5 μM) at 5 d (dashed lines outline original size of constructs at 0 d. Scale bar, 1 mm). (B) Construct size quantification of HSC hydrogels subjected to the different treatments at 5 d (N = 12 hydrogels per group from 3 HSC cell strains with 4 experimental replicates per HSC cell strain). (C) Cell viability quantification of HSC hydrogels subjected to the different treatments at 5 d (N = 12 hydrogels per group from 3 HSC cell strains with 4 experimental replicates per HTM cell strain). Symbols with different colors represent different cell strains. The bars and error bars indicate Mean ± SD. Significance was determined by two-way ANOVA using multiple comparisons tests (****$p<0.0001$).

Discussion

The profibrotic cytokine TGFβ2 is a key contributor to outflow tissue dysfunction in POAG [10, 19]. TGFβ2 has been shown to increase the deposition of ECM material in the JCT-TM beneath the SC inner wall endothelium and contract the SC [26, 27, 30]. Most *in vitro* studies to date investigating the effects of TGFβ2 on outflow cell dysfunction have focused on TM cells [26, 30, 46]. In contrast, the contributions of TGFβ2 to SC cell pathobiology are considerably less well understood. A recent multi-ethnic genome wide meta-analysis identified *YAP1* as a potential genetic risk factor for POAG, implicating that YAP (and perhaps TAZ by association) may play a critical role in glaucoma pathogenesis [40]. We have shown that TGFβ2 upregulates YAP/TAZ activity in HTM cells cultured atop or within ECM hydrogels [26]. Here, our aim was to elucidate mechanisms governing YAP/TAZ modulation in HSC cells in response to TGFβ2 by culturing cells on a tissue-mimetic ECM substrate.

Glaucomatous SC cells isolated from POAG eyes exhibit higher levels of F-actin compared to normal cells [15]. Consistent with this observation, we found that TGFβ2 significantly increased F-actin fibers in HSC cells (**Fig. 2B,C**). It has been extensively reported that the glaucoma-associated stressors dexamethasone and TGFβ2 stimulate the formation of cross-linked actin networks (CLANs) in HTM cells [49-52]. Yet, we did not observe TGFβ2-induced CLANs in HSC cells. A number of signaling pathways including Smad, Wnt, ROCK and ERK have been shown to modulate CLAN formation in HTM cells [53]. Further research will be necessary to investigate the specific contribution of these important signaling pathways in HSC cell pathobiology in the context of cytoskeletal homeostasis.

The transcriptional coactivators YAP and TAZ play important roles in mechanotransduction and POAG pathogenesis [40, 41]. Recently, we showed that activity of YAP/TAZ is upregulated in HTM cells under diverse simulated glaucomatous conditions [26]. However, the mechanisms underlying YAP/TAZ signaling in HSC cells influenced by TGFβ2 remain to be elucidated. We here demonstrated that TGFβ2 increased YAP/TAZ activity in HSC cells, which was potently attenuated by actin cytoskeleton relaxation using Y27632 or actin depolymerization using Lat B (**Fig. 3**). This suggests that actin integrity is required for YAP/TAZ activation in HSC cells. Moreover, we found that a 30 min treatment of Lat B – necessary to preserve HSC cell viability - was more effective than a 3 d treatment of Y27632 on inducing YAP/TAZ cytoplasmic translocalization. A previous study showed that HTM cells can recover to their initial state after removal of Lat B treatment in a short period of time [54]. It would be worthwhile to further investigate whether Y27632/Lat B-reduced YAP/TAZ activity could be reversed with the treatments withheld.

Endothelial-to-mesenchymal transition (EndMT) is a process whereby endothelial cells undergo a series of molecular events, such as increased expression of αSMA, fibronectin, vimentin, and collagen types I and III, that lead to a change in phenotype toward mesenchymal-like cells [55, 56]. TGFβ has been shown to induce EndMT, which can contribute to various fibrotic diseases and cancers [56-59]. In a previous study, it was shown that TGFβ2 stimulated EndMT of HSC cells cultured on top of a synthetic biomaterial; downregulation of endothelial cell markers and upregulation of mesenchymal makers were noted [60]. Consistent with this, we showed that TGFβ2 induced EndMT of HSC cells cultured atop tissue-mimetic ECM hydrogels, as indicated by increased expression of αSMA and fibronectin (**Fig. 2D,E, Fig. 4A-D**). Importantly, we found that TGFβ2-induced EndMT was partially blocked by pharmacologic YAP/TAZ inhibition with

VP treatment (**Fig. 4A-D**). Moreover, TAP/TAZ inhibition decreased TGFβ2-induced expression of TGM2 (**Suppl. Fig. 1E,F**), which crosslinks fibronectin and thereby stiffens the ECM [61]. This suggests that YAP/TAZ inhibition may decrease ECM stiffness to improve aqueous humor outflow. Therefore, targeting YAP/TAZ signaling in the SC endothelium to inhibit EndMT is an intriguing strategy for managing ocular hypertension.

HSC cells are highly contractile [3]. In fact, we found that HSC cells were even more contractile than HTM cells using our ECM hydrogel system (**Fig. 5A**). Actomyosin, the actin-myosin complex, regulates cell contractility in various cell types [62]. HSC cells in absence of any treatment exhibited qualitatively lower levels of actin fibers compared to HTM cells when cultured atop our ECM hydrogels. Therefore, we speculate that the higher degree of HSC cell contractility could stem from upregulated activity of myosin II, which is responsible for producing contraction force [63]. Myosin II activity is primarily regulated by phosphorylation of MLC; this process is mediated by myosin light chain kinase (MLCK) and myosin phosphatase [64]. Importantly, MLCK inhibition has been shown to decrease IOP in rabbit eyes [65]. Blebbistatin, a pharmacologic inhibitor of myosin II adenosine triphosphatase activity, increases outflow facility via blocking the binding of myosin to actin [66]. Futures studies would be necessary to investigate in greater detail the role of myosin II activity and myosin-actin interactions in HSC cell biology.

Consistent with our observation on HTM cells, TGFβ2-treated HSC cells exhibited elevated levels of cell contractility-related molecules (i.e., αSMA, F-actin and p-MLC), which correlated with increased HSC hydrogel contraction. Importantly, this TGFβ2-induced pathologic process was potently attenuated by pharmacologic YAP/TAZ inhibition (**Fig. 4C-H, Fig. 5B-D**). Previous studies showed that outflow resistance is modulated by SC cell stiffness, which is directly

474 correlated with their contractility status [14, 67]. It would be worthwhile to further investigate the
475 effects of YAP/TAZ inhibition on HSC cell stiffness.

476 In conclusion, by culturing HSC cells on tissue-mimetic ECM hydrogels, we demonstrated that
477 TGFβ2 drives actin stress fiber formation to upregulate YAP/TAZ activity, and that YAP/TAZ
478 inhibition reduces HSC cell contractility, which may positively affect cell stiffness and outflow
479 resistance. Our findings provide new evidence for a pathologic role of YAP/TAZ hyperactivation
480 in HSC cell pathobiology in glaucoma, and suggest that pharmacologic YAP/TAZ inhibition has
481 promising potential to improve outflow tissue dysfunction.

482

483 **Disclosure**

484 The authors report no conflicts of interest.

485

486 **Funding**

487 This project was supported in part by National Institutes of Health grants R01EY022359
488 and P30EY005722 (W.D.S.) and K08EY031755 (P.S.G), an American Glaucoma Society Young
489 Clinician Scientist Award (to P.S.G.), a Syracuse University BioInspired Seed Grant (to S.H.),
490 unrestricted grants to SUNY Upstate Medical University Department of Ophthalmology and
491 Visual Sciences from Research to Prevent Blindness (RPB) and from Lions Region 20-Y1, and
492 RPB Career Development Awards (to P.S.G. and S.H.).

493

494

Acknowledgments

We thank Dr. Robert W. Weisenthal and the team at Specialty Surgery Center of Central New York for assistance with corneal rim specimens. We also thank Dr. Nasim Annabi at the University of California – Los Angeles for providing the KCTS-ELP, Dr. Alison Patteson at Syracuse University for rheometer access, and Drs. Audrey M. Bernstein and Mariano S. Viapiano at SUNY Upstate Medical University for imaging support. **Author contributions:** H.L., K.M.P., W.D.S., P.S.G., and S.H. designed all experiments, collected, analyzed, and interpreted the data. K.M.P. and W.D.S. provided the HSC reference cells. H.L. and S.H. wrote the manuscript. All authors commented on and approved the final manuscript. P.S.G. and S.H. conceived and supervised the research. **Data and materials availability:** All data needed to evaluate the conclusions in the paper are present in the paper and/or the Supplementary Materials. Additional data related to this paper may be requested from the authors.

References

1. Ashpole NE, Overby DR, Ethier CR, Stamer WD. Shear stress-triggered nitric oxide release from Schlemm's canal cells. *Investigative ophthalmology & visual science* 2014;55:8067-8076.
2. Dautriche CN, Tian Y, Xie Y, Sharfstein ST. A Closer Look at Schlemm's Canal Cell Physiology: Implications for Biomimetics. *J Funct Biomater* 2015;6:963-985.
3. Stamer WD, Braakman ST, Zhou EH, et al. Biomechanics of Schlemm's canal endothelium and intraocular pressure reduction. *Prog Retin Eye Res* 2015;44:86-98.
4. Ethier CR. The inner wall of Schlemm's canal. *Exp Eye Res* 2002;74:161-172.
5. Stamer WD, Roberts BC, Howell DN, Epstein DL. Isolation, culture, and characterization of endothelial cells from Schlemm's canal. *Invest Ophthalmol Vis Sci* 1998;39:1804-1812.
6. Gong H, Francis AW. Schlemm s Canal and Collector Channels as Therapeutic Targets. 2014.
7. Tamm ER. The trabecular meshwork outflow pathways: structural and functional aspects. *Exp Eye Res* 2009;88:648-655.
8. Tamm ER, Braunger BM, Fuchshofer R. Intraocular Pressure and the Mechanisms Involved in Resistance of the Aqueous Humor Flow in the Trabecular Meshwork Outflow Pathways. *Prog Mol Biol Transl Sci* 2015;134:301-314.

9. Brubaker RF. Flow of aqueous humor in humans [The Friedenwald Lecture]. *Invest Ophthalmol Vis Sci* 1991;32:3145-3166.
10. Quigley HA. Open-angle glaucoma. *N Engl J Med* 1993;328:1097-1106.
11. Quigley HA, Broman AT. The number of people with glaucoma worldwide in 2010 and 2020. *Br J Ophthalmol* 2006;90:262-267.
12. Kwon YH, Fingert JH, Kuehn MH, Alward WL. Primary open-angle glaucoma. *N Engl J Med* 2009;360:1113-1124.
13. Tham YC, Li X, Wong TY, Quigley HA, Aung T, Cheng CY. Global prevalence of glaucoma and projections of glaucoma burden through 2040: a systematic review and meta-analysis. *Ophthalmology* 2014;121:2081-2090.
14. Overby DR, Zhou EH, Vargas-Pinto R, et al. Altered mechanobiology of Schlemm's canal endothelial cells in glaucoma. *Proc Natl Acad Sci U S A* 2014;111:13876-13881.
15. Kelly RA, Perkumas KM, Campbell M, et al. Fibrotic Changes to Schlemm's Canal Endothelial Cells in Glaucoma. *Int J Mol Sci* 2021;22.
16. Tian YI, Zhang X, Torrejon K, et al. A bioengineering approach to Schlemm's canal-like stem cell differentiation for in vitro glaucoma drug screening. *Acta Biomater* 2020;105:203-213.
17. Rao PV, Deng PF, Kumar J, Epstein DL. Modulation of aqueous humor outflow facility by the Rho kinase-specific inhibitor Y-27632. *Invest Ophthalmol Vis Sci* 2001;42:1029-1037.
18. Kumar J, Epstein DL. Rho GTPase-mediated cytoskeletal organization in Schlemm's canal cells play a critical role in the regulation of aqueous humor outflow facility. *J Cell Biochem* 2011;112:600-606.
19. Fuchshofer R, Tamm ER. Modulation of extracellular matrix turnover in the trabecular meshwork. *Experimental Eye Research* 2009;88:683-688.
20. Granstein RD, Staszewski R, Knisely TL, et al. Aqueous humor contains transforming growth factor-beta and a small (less than 3500 daltons) inhibitor of thymocyte proliferation. *J Immunol* 1990;144:3021-3027.
21. Inatani M, Tanihara H, Katsuta H, Honjo M, Kido N, Honda Y. Transforming growth factor-beta 2 levels in aqueous humor of glaucomatous eyes. *Graefes Arch Clin Exp Ophthalmol* 2001;239:109-113.
22. Agarwal P, Daher AM, Agarwal R. Aqueous humor TGF-β2 levels in patients with open-angle glaucoma: A meta-analysis. *Molecular vision* 2015;21:612-620.
23. Kasetti RB, Maddineni P, Patel PD, Searby C, Sheffield VC, Zode GS. Transforming growth factor β2 (TGFβ2) signaling plays a key role in glucocorticoid-induced ocular hypertension. *J Biol Chem* 2018;293:9854-9868.
24. Ochiai Y, Ochiai H. Higher concentration of transforming growth factor-beta in aqueous humor of glaucomatous eyes and diabetic eyes. *Jpn J Ophthalmol* 2002;46:249-253.
25. Picht G, Welge-Luessen U, Grehn F, Lutjen-Drecoll E. Transforming growth factor beta 2 levels in the aqueous humor in different types of glaucoma and the relation to filtering bleb development. *Graefes Arch Clin Exp Ophthalmol* 2001;239:199-207.
26. Li H, Raghunathan V, Stamer WD, Ganapathy PS, Herberg S. Extracellular Matrix Stiffness and TGFβ2 Regulate YAP/TAZ Activity in Human Trabecular Meshwork Cells. *Frontiers in Cell and Developmental Biology* 2022;10.
27. Gottanka J, Chan D, Eichhorn M, Lutjen-Drecoll E, Ethier CR. Effects of TGF-beta2 in perfused human eyes. *Invest Ophthalmol Vis Sci* 2004;45:153-158.

28. Han H, Wecker T, Grehn F, Schlunck G. Elasticity-Dependent Modulation of TGF-β Responses in Human Trabecular Meshwork Cells. *Investigative Ophthalmology & Visual Science* 2011;52:2889-2896.
29. Pattabiraman PP, Rao PV. Mechanistic basis of Rho GTPase-induced extracellular matrix synthesis in trabecular meshwork cells. *Am J Physiol Cell Physiol* 2010;298:C749-763.
30. Li H, Henty-Ridilla JL, Bernstein AM, Ganapathy PS, Herberg S. TGFβ2 regulates human trabecular meshwork cell contractility via ERK and ROCK pathways with distinct signaling crosstalk dependent on the culture substrate. *Current Eye Research* 2022;1-41.
31. Fuchshofer R, Welge-Lussen U, Lütjen-Drecoll E. The effect of TGF-beta2 on human trabecular meshwork extracellular proteolytic system. *Exp Eye Res* 2003;77:757-765.
32. Fuchshofer R, Tamm ER. The role of TGF-β in the pathogenesis of primary open-angle glaucoma. *Cell Tissue Res* 2012;347:279-290.
33. Welge-Lüßen U, May CA, Lütjen-Drecoll E. Induction of Tissue Transglutaminase in the Trabecular Meshwork by TGF-β1 and TGF-β2. *Investigative Ophthalmology & Visual Science* 2000;41:2229-2238.
34. Moroishi T, Hansen CG, Guan K-L. The emerging roles of YAP and TAZ in cancer. *Nature Reviews Cancer* 2015;15:73-79.
35. Plouffe SW, Hong AW, Guan K-L. Disease implications of the Hippo/YAP pathway. *Trends in Molecular Medicine* 2015;21:212-222.
36. Polansky JR, Fauss DJ, Zimmerman CC. Regulation of TIGR/MYOC gene expression in human trabecular meshwork cells. *Eye (Lond)* 2000;14 (Pt 3B):503-514.
37. Zhao B, Wei X, Li W, et al. Inactivation of YAP oncoprotein by the Hippo pathway is involved in cell contact inhibition and tissue growth control. *Genes Dev* 2007;21:2747-2761.
38. Silver JS, Günay KA, Cutler AA, et al. Injury-mediated stiffening persistently activates muscle stem cells through YAP and TAZ mechanotransduction. *Sci Adv* 2021;7.
39. Low BC, Pan CQ, Shivashankar GV, Bershadsky A, Sudol M, Sheetz M. YAP/TAZ as mechanosensors and mechanotransducers in regulating organ size and tumor growth. *FEBS Lett* 2014;588:2663-2670.
40. Gharahkhani P, Jorgenson E, Hysi P, et al. Genome-wide meta-analysis identifies 127 open-angle glaucoma loci with consistent effect across ancestries. *Nat Commun* 2021;12:1258.
41. Dupont S, Morsut L, Aragona M, et al. Role of YAP/TAZ in mechanotransduction. *Nature* 2011;474:179-183.
42. Boopathy GTK, Hong W. Role of Hippo Pathway-YAP/TAZ Signaling in Angiogenesis. *Frontiers in Cell and Developmental Biology* 2019;7.
43. Li H, Bagué T, Kirschner A, et al. A tissue-engineered human trabecular meshwork hydrogel for advanced glaucoma disease modeling. *Exp Eye Res* 2021;205:108472.
44. Perkumas KM, Stamer WD. Protein markers and differentiation in culture for Schlemm's canal endothelial cells. *Exp Eye Res* 2012;96:82-87.
45. Keller KE, Bhattacharya SK, Borras T, et al. Consensus recommendations for trabecular meshwork cell isolation, characterization and culture. *Exp Eye Res* 2018;171:164-173.
46. Torrejon KY, Papke EL, Halman JR, et al. TGFβ2-induced outflow alterations in a bioengineered trabecular meshwork are offset by a rho-associated kinase inhibitor. *Sci Rep* 2016;6:38319.
47. Das A, Fischer RS, Pan D, Waterman CM. YAP Nuclear Localization in the Absence of Cell-Cell Contact Is Mediated by a Filamentous Actin-dependent, Myosin II- and Phospho-YAP-

616 independent Pathway during Extracellular Matrix Mechanosensing*. *Journal of Biological*
617 *Chemistry* 2016;291:6096-6110.
618 48. Liu-Chittenden Y, Huang B, Shim JS, et al. Genetic and pharmacological disruption of
619 the TEAD-YAP complex suppresses the oncogenic activity of YAP. *Genes Dev* 2012;26:1300-
620 1305.
621 49. Montecchi-Palmer M, Bermudez JY, Webber HC, Patel GC, Clark AF, Mao W. TGFβ2
622 Induces the Formation of Cross-Linked Actin Networks (CLANs) in Human Trabecular
623 Meshwork Cells Through the Smad and Non-Smad Dependent Pathways. *Investigative*
624 *ophthalmology & visual science* 2017;58:1288-1295.
625 50. Clark AF, Brotchie D, Read AT, et al. Dexamethasone alters F-actin architecture and
626 promotes cross-linked actin network formation in human trabecular meshwork tissue. *Cell Motil*
627 *Cytoskeleton* 2005;60:83-95.
628 51. Yuan Y, Call MK, Yuan Y, et al. Dexamethasone Induces Cross-Linked Actin Networks
629 in Trabecular Meshwork Cells Through Noncanonical Wnt Signaling. *Investigative*
630 *Ophthalmology & Visual Science* 2013;54:6502-6509.
631 52. Filla MS, Schwinn MK, Nosie AK, Clark RW, Peters DM. Dexamethasone-associated
632 cross-linked actin network formation in human trabecular meshwork cells involves beta3 integrin
633 signaling. *Invest Ophthalmol Vis Sci* 2011;52:2952-2959.
634 53. Zhang YE. Non-Smad pathways in TGF-β signaling. *Cell Research* 2009;19:128-139.
635 54. McKee CT, Wood JA, Shah NM, et al. The effect of biophysical attributes of the ocular
636 trabecular meshwork associated with glaucoma on the cell response to therapeutic agents.
637 *Biomaterials* 2011;32:2417-2423.
638 55. Choi KJ, Nam J-K, Kim J-H, Choi S-H, Lee Y-J. Endothelial-to-mesenchymal transition
639 in anticancer therapy and normal tissue damage. *Exp Mol Med* 2020;52:781-792.
640 56. Ma J, Sanchez-Duffhues G, Goumans M-J, ten Dijke P. TGF-β-Induced Endothelial to
641 Mesenchymal Transition in Disease and Tissue Engineering. *Frontiers in Cell and*
642 *Developmental Biology* 2020;8.
643 57. Clere N, Renault S, Corre I. Endothelial-to-Mesenchymal Transition in Cancer. *Frontiers*
644 *in Cell and Developmental Biology* 2020;8.
645 58. Zeisberg EM, Potenta SE, Sugimoto H, Zeisberg M, Kalluri R. Fibroblasts in kidney
646 fibrosis emerge via endothelial-to-mesenchymal transition. *J Am Soc Nephrol* 2008;19:2282-
647 2287.
648 59. Pérez L, Muñoz-Durango N, Riedel CA, et al. Endothelial-to-mesenchymal transition:
649 Cytokine-mediated pathways that determine endothelial fibrosis under inflammatory conditions.
650 *Cytokine Growth Factor Rev* 2017;33:41-54.
651 60. Dautriche CN, Szymanski D, Kerr M, et al. A biomimetic Schlemm's canal inner wall: A
652 model to study outflow physiology, glaucoma pathology and high-throughput drug screening.
653 *Biomaterials* 2015;65:86-92.
654 61. Akimov SS, Krylov D, Fleischman LF, Belkin AM. Tissue transglutaminase is an
655 integrin-binding adhesion coreceptor for fibronectin. *The Journal of cell biology* 2000;148:825-
656 838.
657 62. Murrell M, Oakes PW, Lenz M, Gardel ML. Forcing cells into shape: the mechanics of
658 actomyosin contractility. *Nat Rev Mol Cell Biol* 2015;16:486-498.
659 63. Kolega J. The role of myosin II motor activity in distributing myosin asymmetrically and
660 coupling protrusive activity to cell translocation. *Mol Biol Cell* 2006;17:4435-4445.

64. Fukata Y, Amano M, Kaibuchi K. Rho-Rho-kinase pathway in smooth muscle contraction and cytoskeletal reorganization of non-muscle cells. *Trends Pharmacol Sci* 2001;22:32-39.
65. Honjo M, Inatani M, Kido N, et al. A myosin light chain kinase inhibitor, ML-9, lowers the intraocular pressure in rabbit eyes. *Exp Eye Res* 2002;75:135-142.
66. Zhang M, Rao PV. Blebbistatin, a Novel Inhibitor of Myosin II ATPase Activity, Increases Aqueous Humor Outflow Facility in Perfused Enucleated Porcine Eyes. *Investigative Ophthalmology & Visual Science* 2005;46:4130-4138.
67. Zhou EH, Krishnan R, Stamer WD, et al. Mechanical responsiveness of the endothelial cell of Schlemm's canal: scope, variability and its potential role in controlling aqueous humour outflow. *J R Soc Interface* 2012;9:1144-1155.